NANO LETTERS

Letter

pubs.acs.org/NanoLett

Controlling Electron Overflow in Phosphor-Free InGaN/GaN Nanowire White Light-Emitting Diodes

Hieu Pham Trung Nguyen,[†] Kai Cui,[†] Shaofei Zhang,[†] Mehrdad Djavid,[†] Andreas Korinek,[‡] Gianluigi A. Botton,[‡] and Zetian Mi*,[†]

[†]Department of Electrical and Computer Engineering, McGill University, 3480 University Street, Montreal, Quebec H3A 2A7, Canada

[‡]Canadian Centre for Electron Microscopy and Brockhouse Institute for Materials Research, McMaster University, 1280 Main Street West, Hamilton, Ontario

Supporting Information

ABSTRACT: We have investigated for the first time the impact of electron overflow on the performance of nanowire light-emitting diodes (LEDs) operating in the entire visible spectral range, wherein intrinsic white light emission is achieved from self-organized InGaN quantum dots embedded in defect-free GaN nanowires on a single chip. Through detailed temperature-dependent electroluminescence and simulation studies, it is revealed that electron leakage out of the device active region is primarily responsible for efficiency degradation in such nanowire devices, which in conjunction with the presence of nonradiative surface recombination largely determines the unique emission characteristics of nanowire light-emitting diodes. We have further demonstrated that electron overflow in nanowire LEDs can be effectively prevented with the incorporation of a p-doped AlGaN electron blocking layer, leading to the achievement of phosphor-free white light-emitting diodes that can exhibit for the first time virtually zero efficiency droop for injection currents up to ~2200 A/cm^2. This study also provides unambiguous evidence that Auger recombination is not the primary mechanism responsible for efficiency droop in GaN-based nanowire light-emitting diodes.

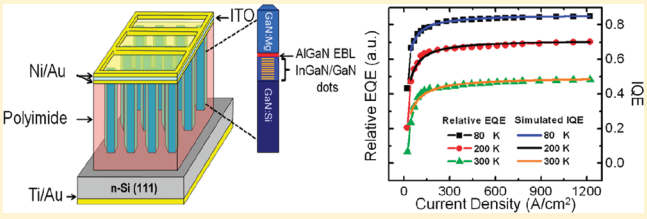

KEYWORDS: *Nanowire, quantum dot, InGaN, light-emitting diodes, electron overflow, Auger recombination*

One of the grand challenges for future solid-state lighting is the development of all semiconductor-based white light-emitting diodes (LEDs), consisting of monolithically integrated blue, green, and red devices, that can exhibit ultrahigh-efficiency, long-term reliability, and tunable color emission. The achievement of such devices using conventional GaN-based planar heterostructures, however, has been severely limited by their low efficiency and efficiency droop in the green-to-red spectral range, which has been explained by the presence of polarization fields,[1,2] Auger recombination,[3,4] poor hole transport,[5] defects/dislocations,[6,7] and/or electron leakage and overflow.[1,8−10] In this regard, significant progress has been made in nanowire white LEDs with the active regions consisting of well/disk-in-a-wire,[11,12] core/shell,[13] ternary nanowire,[14,15] and dot-in-a-wire nanoscale heterostructures.[16,17] In such nanowire devices, mechanisms that may contribute to efficiency degradation, including dislocations, polarization fields, as well as the associated quantum-confined Stark effect (QCSE),[1,18−20] can be greatly minimized.[16,21,22] Compared to conventional planar heterostructures, however, the performance of such nanoscale LEDs is more susceptible to electron leakage out of the device active region due to the presence of large densities of states/defects along the wire surface and the one-dimensional carrier transport process.[23−25] The resulting carrier loss and nonradiative carrier recombination severely limit the maximum quantum efficiency achievable at high current injection levels. To date, however, the presence of electron overflow and its predominant effect on the performance of nanowire LEDs has not been reported. Additionally, it has remained a subject of intensive debate on the role of Auger recombination in the performance of GaN-based LEDs.[3,26−28]

In this paper, we have investigated for the first time the impact of electron overflow on the performance of nanowire LEDs operating in the entire visible spectral range. Intrinsic white light emission is achieved by incorporating self-organized InGaN quantum dots with controlled compositions and sizes in defect-free GaN nanowires on a single chip. The role of electron overflow on the performance limit of such nanoscale LEDs has been elucidated by characterizing, both experimentally and theoretically, the current-dependent electroluminescence emission of an InGaN/GaN test quantum well embedded between the quantum dot active region and the p-GaN, wherein electrons escaping the quantum dot active region can be correlated with the optical emission from the test well. It is measured that electron overflow is present even under

Received: November 2, 2011
Revised: January 24, 2012
Published: January 27, 2012

   dx.doi.org/10.1021/nl203860b | *Nano Lett.* 2012, 12, 1317−1323

relatively low-injection conditions (below the onset of efficiency droop), which in conjunction with the nonradiative carrier recombination related to the surface states/defects largely determines the unique emission characteristics of nanowire LEDs. Moreover, we have demonstrated that with the incorporation of a p-doped AlGaN electron blocking layer between the active region and the p-GaN section electron overflow can be effectively prevented. The resulting white LEDs can exhibit for the first time virtually no efficiency droop up to ~2200 A/cm^2, thereby providing a highly promising approach for future high-power, all semiconductor-based solid-state lighting. This study also provides unambiguous evidence that Auger recombination is not likely the primary mechanism responsible for efficiency droop in GaN-based nanowire LEDs.

In this experiment, vertically aligned InGaN/GaN dot-in-a-wire heterostructures were grown on Si(111) substrates by radio frequency plasma-assisted molecular beam epitaxy under nitrogen rich condition. The device active region contains 10 vertically coupled InGaN/GaN quantum dots. Each InGaN quantum dot has a height of ~3 nm and is capped by ~3 nm GaN layer. Detailed growth conditions for such dot-in-a-wire nanoscale heterostructures are described in previous publications.[16,17] Figure 1a shows the schematic of a typical dot-in-a-wire LED device. To investigate the electron overflow phenomena, an InGaN/GaN dot-in-a-wire LED heterostructure with the incorporation of a p-doped InGaN/GaN test quantum well between the device active region and p-GaN section is grown (LED I shown in Figure 1b). In this design, electrons leaking out of the quantum dots can recombine with holes in the test well, which has smaller In compositions than that of the InGaN/GaN quantum dots. The resulting optical emission can therefore be used to evaluate electron overflow in nanowire LEDs. Additionally, we have designed nanoscale LEDs (LED II) with the incorporation of a p-doped AlGaN electron blocking layer between the LED active region and the InGaN test quantum well in order to study its effect in preventing electron overflow.[29,30] Finally, a third LED device that consists of a p-doped AlGaN electron blocking layer, but without the InGaN test well, is also investigated. The three nanowire LED designs are schematically shown in Figure 1b. The flat energy band diagrams along the nanowire axial dimension are also shown in the insets. Illustrated in Figure 1c are the photoluminescence spectra of such nanowire LEDs measured at room temperature. The peak at ~550 nm is related to the emission from the quantum dot active region, while the peak at ~430 nm is due to the presence of an InGaN test well, which can be measured for the first and second nanowire LEDs.

The dot-in-a-wire LEDs exhibit excellent structural properties. Shown in Figure 2a is a 45° tilted scanning electron microscopy image of the dot-in-a-wire LED heterostructures grown on Si(111) substrates. The wire diameters and densities are in the ranges of 40−100 nm and ~1 × 10^{10} cm^{-2}, respectively. The nanowires are vertically aligned to the substrate and exhibit a high degree of size uniformity. A CM200 microscope with acceleration voltage of 200 kV was used to obtain bright-field transmission electron microscopy (TEM) images. A Titan 80-300 scanning transmission electron microscope (STEM) equipped with an aberration corrector for the image-forming lens was used for annular dark-field imaging and energy dispersive X-ray spectrometry (EDXS) analysis with an electron beam of approximately 0.2 nm in diameter. The Ga and Al K_α lines and In L_α line were used for the EDXS microanalysis. The TEM image for LED II is shown in Figure 2b, wherein the 10 InGaN/GaN quantum dots, the AlGaN electron-blocking layer, as well as the InGaN quantum well are identified. There are no extended defects, such as misfit dislocations and stacking faults observed in the view of the current images. InGaN/GaN quantum dots are positioned in the center of the nanowires, due to the strain-induced self-organization. In order to confirm the existence of each region and obtain an estimation of the elemental variations, EDXS analysis together with the annular dark-field image were also performed. The EDXS line profile showing the signal variations of Ga, In, and Al across different regions along the growth direction of LED II are displayed in Figure 2c. The variation of In signal reveals the existence of InGaN quantum dots and InGaN quantum well. With the Ga signal from GaN region as a reference and also considering the thickness of the dots along the electron beam traveling path, the maximum In is estimated as ~50% constituting group III elements for the dots. Although from simple inspection of the profiles, the In composition of the InGaN quantum well appears higher than the one of the quantum dots, we cannot quantitatively compare the composition of the two structures at this point. Because of

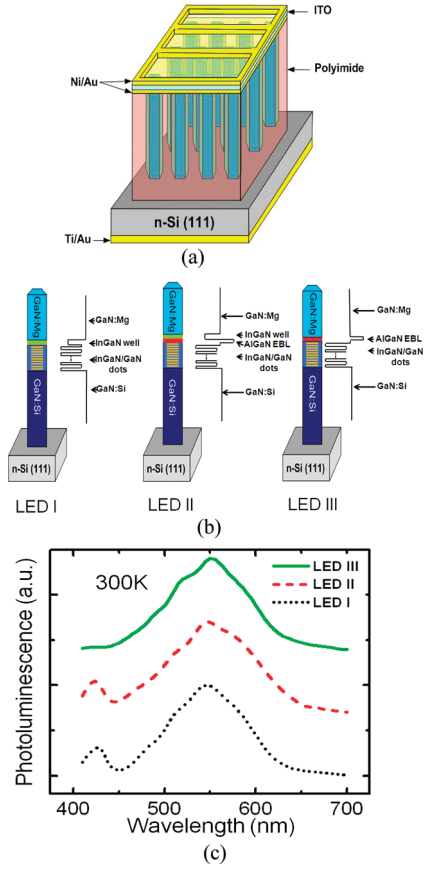

Figure 1. (a) Schematic illustration of InGaN/GaN dot-in-a-wire LEDs grown on Si(111) substrates. (b) Illustration of the three LED designs. From left to right: InGaN/GaN dot-in-a-wire LEDs with the incorporation of an InGaN test well (LED I), an AlGaN electron blocking layer (EBL) and an InGaN test well (LED II), and an AlGaN electron blocking layer (LED III) between the quantum dot active region and the p-GaN section. Flat energy band diagrams for the three LED structures are illustrated in the insets. (c) Room-temperature photoluminescence spectra of the three LED device heterostructures. The emission peak at ~430 nm is due to the presence of the InGaN test well, which can be clearly measured for LEDs I and II.

dx.doi.org/10.1021/nl203860b | Nano Lett. 2012, 12, 1317−1323

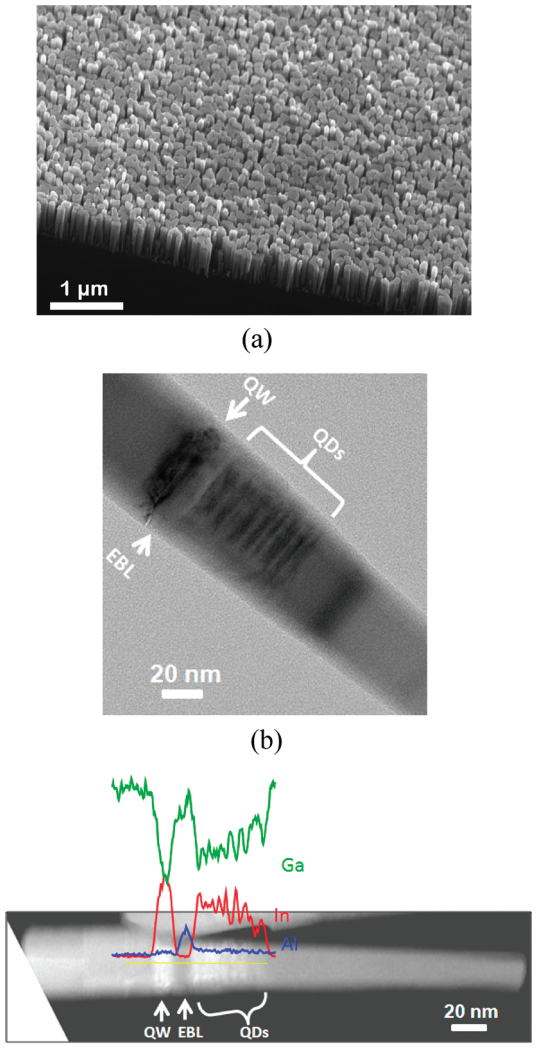

Figure 2. (a) A 45° tilted scanning electron microscopy image of the InGaN/GaN dot-in-a-wire LED heterostructure grown on Si(111) substrates. (b) Bright-field TEM image of InGaN/GaN dot-in-a-wire LED II, wherein the InGaN quantum well (QW), quantum dots (QDs), and AlGaN electron blocking layer (EBL) are identified. (c) Annular dark-field STEM image and EDXS signals for In, Ga, and Al of LED II.

the much thinner width of the dots, the finite spatial resolution for EDXS analysis, and the possible tilting of the dots away from the electron beam incident direction, the absolute In intensities cannot be directly compared in the two structures and further work is in progress to fully quantify the composition. Nevertheless, qualitative information on the presence of the In and Al has been extracted to confirm the presence of the key components of the device. From the Al signal profile, the AlGaN electron blocking layer is observed between the dot and well region for LED II, shown in Figure 2c. The thickness of the electron blocking layer is about 8 nm. In this experiment, the Al composition of the electron blocking layer is varied from ∼8 to 20%. The quality of the nanowire LEDs has been confirmed by the very high internal quantum efficiency (∼ 30 to 60%) measured at room temperature.[16,17,31]

The nanowire LED fabrication process includes the following steps. First, a polyimide resist layer was spin-coated to fully cover the nanowires, followed by O_2 plasma etching to expose the top portions of the nanowires. Thin Ni(5 nm)/Au(5 nm) and Ti(20 nm)/Au(120 nm) metal layers were then deposited on the nanowire surface and the backside of the Si substrate to serve as p- and n-metal contacts, respectively. A 150 nm indium tin oxide (ITO) layer was coated on the device top surface to serve as a transparent electrode and current spreading layer. The fabricated devices with Ti/Au and Ni/Au contacts were annealed at ∼500 °C for 1 min in nitrogen ambient, and the complete devices with ITO contacts were annealed at 300 °C for 1 h in vacuum. LEDs with chip areas of ∼300 × 300 μm^2 were fabricated and measured.

Emission characteristics of the InGaN/GaN dot-in-a-wire LEDs were studied. Electroluminescence was measured under pulsed biasing condition at various temperatures. Junction heating is minimized by using a low (∼ 0.1%) duty cycle. Figure 3a shows the normalized electroluminescence spectra of LED I measured under various injection currents at room temperature, which incorporates an InGaN test well between the device active region and the p-GaN. The peak at ∼550 nm is related to the emission from the quantum dot active region, which agrees well with the photoluminescence measurements shown in Figure 1c. However, with increasing current it is seen that the emission at ∼430 nm becomes progressively stronger, which is attributed to the carrier recombination in the InGaN/GaN test well. This observation confirms that injected electrons can escape from the quantum dot active region and subsequently recombine with holes in the InGaN test well. Shown in Figure 3b is the derived relative external quantum efficiency (in arbitrary units) related to the electroluminescence emission from the quantum dot active region as well as that from the test well measured at room temperature. It is seen that for the emission from the test well the quantum efficiency continuously increases with current, which can be explained by the increased electron overflow and therefore enhanced emission from the test well region with increasing current. For the emission of the quantum dot active region, the relative external quantum efficiency reaches its peak value at ∼300−400 A/cm^2 and shows a continuous drop (∼6%) with further increasing current up to 1100 A/cm^2, which can be explained by the enhanced electron overflow at high injection conditions. It may also be noticed that electron overflow is appreciable below such injection levels, evidenced by the presence of emission peak from the test well at an injection current of ∼300 A/cm^2.

It is further measured that electron overflow is relatively enhanced with decreasing temperature. Shown in Figure 3(c), the emission intensity from the test well becomes comparable to that from the quantum dots when measured under an injection current of ∼450 A/cm^2 at low temperatures (∼ 80K), while its peak intensity is only ∼10% of that from the dots when measured at the same injection current at room temperature. Consequently, the quantum efficiency related to the optical emission from the quantum dot active region shows a more severe drop with decreasing temperature. Illustrated in Figure 3(d), the estimated efficiency drop is ∼6%, 10%, and 21% for measurements performed under an injection current of ∼1,100 A/cm^2 at 300 K, 200 K, and 80 K, respectively. The increased electron overflow at low temperatures is consistent with recent theoretical studies.[32] At low temperatures, the hole concentration in the p-GaN region is drastically reduced, due to the large activation energy for Mg dopant, thereby leading to reduced hole injection efficiency and further enhanced electron overflow. It is also observed that, with decreasing temperature,

dx.doi.org/10.1021/nl203860b | Nano Lett. 2012, 12, 1317−1323

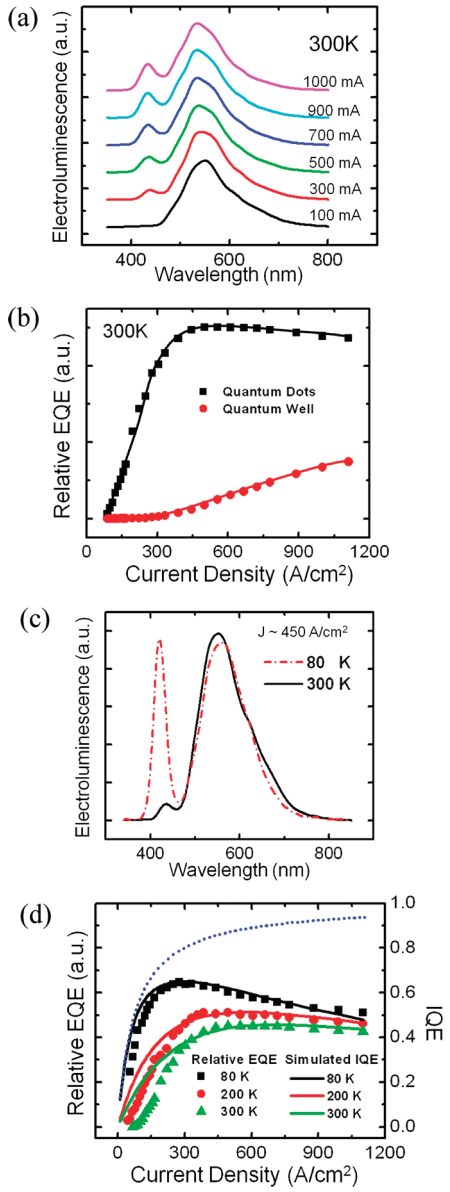

Figure 3. (a) Normalized electroluminescence spectra of LED I under various injection currents. The peak at ~550 nm is related to the emission from the quantum dot active region, while the peak at ~430 nm is related to the emission from the InGaN/GaN test quantum well. (b) Variations of the relative external quantum efficiency with injection current for the emission from the quantum dot active region and the test well of LED I measured at room temperature. (c) Normalized electroluminescence spectra of LED I measured at 300 K (solid line) and 80 K (dashed line) under an injection current density of ~450 A/cm^2. (d) Variations of the relative external quantum efficiency (EQE) related to the emission from the quantum dot active region measured at 80, 200, and 300 K. The simulated internal quantum efficiency (IQE) based on the ABF model is also shown for comparison. The dotted blue line is the calculated IQE versus injection current in the absence of any 3rd or higher order carrier loss mechanisms.

the peak quantum efficiency shifts to lower current densities, shown in Figure 3(d), due to the reduced Shockley-Read-Hall recombination as well as the enhanced bimolecular radiative recombination rate.

These phenomena can be well simulated by using the following model for the internal quantum efficiency,

$$\eta_i = \frac{BN^2}{AN + BN^2 + f(N)} \quad (1)$$

where N is the carrier density in the device active region, and A and B are the Shockley-Read-Hall nonradiative recombination and radiative recombination coefficients, respectively.[28,33] $f(N)$ represents for any other higher order effects, including Auger recombination and carrier leakage outside of the device active region, which are generally described by $CN^3 + DN^4$. In this study, D is assumed to be zero. The carrier density (N) is related to the injection current density (J) by:

$$J = qW_{QD}[AN + BN^2 + f(N)] \quad (2)$$

where W_{QD} represents the total thickness (~ 25−30 nm) of the quantum dot active region. Illustrated in Figure 3(d), the measured relative external quantum efficiency at various temperatures can be well simulated using this model. The derived values of (A, B, C) are ~ (2.6×10^8 s^{-1}, 6.0×10^{-10} cm^{3}s^{-1}, 1.0×10^{-28} cm^{6}s^{-1}), (6×10^8 s^{-1}, 4×10^{-10} cm^{3}s^{-1}, 6×10^{-29} cm^{6}s^{-1}), and (7.0×10^8 s^{-1}, 3×10^{-10} cm^{3}s^{-1}, 4.5×10^{-29} cm^{6}s^{-1}) at 80 K, 200 K, and 300 K, respectively. Additionally, it may be noticed that the quantum efficiency of nanowire LEDs generally reaches its peak value at significantly higher current densities (>200 A/cm^2), compared to that (<20 A/cm^2) of conventional InGaN/GaN quantum well blue LEDs.[17,27,31,34,35] This observation is consistent with the simulated Shockley-Read-Hall recombination coefficient (A ~ 7×10^8 s^{-1}) at 300 K in the present nanowire LEDs, which is significantly larger than the values commonly employed in InGaN/GaN quantum well blue LEDs[36−38] and can be partly explained by the significantly enhanced nonradiative surface recombination, due to the very large surface-to-volume ratios of nanowires. The commonly observed surface band bending in GaN nanowires,[39] as well as the inefficient carrier capture by quantum dots due to hot carrier effect,[8,40] may also contribute considerably to the nonradiative carrier recombination on nanowire surfaces. As a consequence, emission characteristics of nanowire LEDs are predominantly determined by surface-related nonradiative carrier recombination under relatively low carrier injection conditions. In the absence of any third or higher order carrier loss mechanisms, it is further expected that the quantum efficiency should display a small, continuous increase under high injection conditions, illustrated as the dotted blue line in Figure 3(d). To date, however, such phenomena have not been observed in nanowire LEDs,[17,27,41] suggesting the presence of electron overflow or any other high order carrier loss mechanisms, which can lead to either an apparently constant quantum efficiency or efficiency droop under high injection currents.

It has been demonstrated that carrier leakage and electron overflow plays a dominant role on the efficiency droop of GaN based planar LEDs,[10,41−43] which is directly related to the ineffective electron confinement,[44] poor hole transport,[5] and even possibly Auger recombination[10] and can be further exasperated by the presence of polarization fields.[1] In this experiment, the more severe efficiency degradation measured at lower temperatures indicates that Auger recombination and Auger-assisted overflow are not likely the primary mechanisms responsible for efficiency droop in nanowire devices, since Auger recombination coefficient (C) generally decreases

dx.doi.org/10.1021/nl203860b | Nano Lett. 2012, 12, 1317−1323

exponentially with decreasing temperature. This study is also consistent with recent results that Auger recombination is drastically reduced in nearly defect-free GaN-based nanowire devices.[27] Further study on the electron overflow is performed by simulating the band-diagram and carrier distribution in the device active region using the advanced LED device simulation software APSYS. With an average In composition of ~20% in the dots, ~ 10% of the injected current density can leak into the p-GaN region under an injection current density of ~1,000 A/cm^2 (see Figure S1 in Supporting Information). However, much more severe electron overflow is expected, due to the highly nonuniform In distribution along the lateral dimension of the dot-in-a-wire structures. More importantly, the current path associated with the near-surface GaN region can contribute significantly to electron overflow in InGaN/GaN dot-in-a-wire LEDs as well (see the inset of Figure S1 in Supporting Information). Simulations were also performed on LED III, wherein a p-doped AlGaN electron blocking layer is incorporated between the quantum dot active region and p-GaN. In this case, electron overflow, through both the quantum dot active region and the near-surface GaN, can be largely eliminated (see Figure S1 in the Supporting Information).[29,30] Detailed studies also suggest that the use of an electron blocking layer can be significantly more effective in preventing electron overflow in InGaN/GaN nanowire LEDs, due to the drastically reduced polarization fields, compared to conventional InGaN/GaN quantum well devices.[10,45,46]

Experimentally, the effectiveness of utilizing an AlGaN electron blocking layer in preventing electron overflow in nanowire LEDs is demonstrated by examining the electroluminescence spectra of LED II, wherein an 8 nm $Al_{0.15}Ga_{0.85}N$ electron blocking layer is incorporated between the quantum dot active region and the InGaN test well. The measurements were performed up to very high injection conditions (~ 1,222 A/cm^2) at 80 K, 200 K, and 300 K, illustrated in Figure 4.

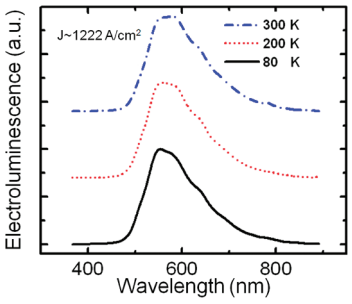

Figure 4. Normalized electroluminescence spectra of LED II measured under an injection current density of ~1,222 A/cm^2 at 80, 200, and 300 K. Emission peak from the InGaN test well is not observed, suggesting the drastically reduced, or the absence of electron overflow in the LED devices with the incorporation of an AlGaN electron blocking layer.

Compared to the photoluminescence results shown in Figure 1(c), however, only emission from the quantum dot active region (λ_{peak} ~ 550 nm) can be observed under electrical injection, and any emission from the test well (~ 430 nm) is absent for measurements performed at various injection conditions and temperatures, which confirms the drastically reduced, or eliminated electron overflow by the AlGaN electron blocking layer.

The performance characteristics of LED III, which consists of ten vertically aligned InGaN/GaN quantum dots and an AlGaN electron blocking layer are subsequently investigated. Variations of the relative external quantum efficiency with injection current are measured at 80 K, 200 K, and 300 K, depicted in Figure 5(a). It is observed that the quantum efficiency first

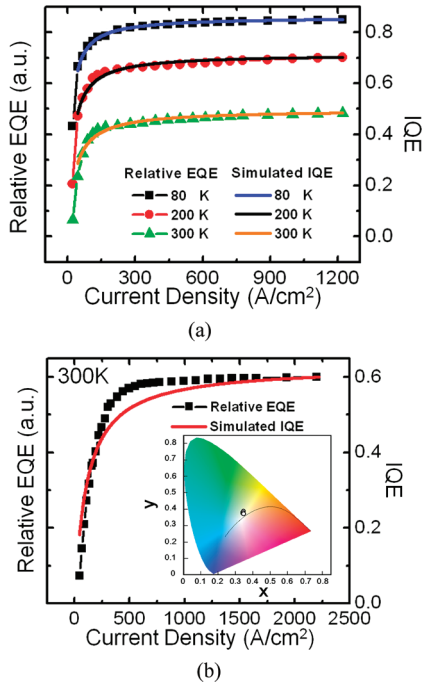

Figure 5. (a) Variations of the measured relative external quantum efficiencies of LED III with injection current at 80 K, 200 K, and 300 K. Variations of the simulated IQE with current using the ABF model show a good agreement with experimental results. (b) Relative external quantum efficiency measured at room temperature for the InGaN/GaN dot-in-a-wire LED with the incorporation of an AlGaN electron blocking layer and p-type modulation doping in the device active region. Shown in the inset is the 1931 Commission International de l'Eclairage chromaticity diagram. The device exhibits highly stable emission characteristics with x and y in the ranges of ~0.33−0.35 and 0.36−0.38, respectively.

shows a significant increase with increasing current, which is directly related to the saturation of defects with increasing carrier density. A very interesting phenomenon, however, is that the quantum efficiency displays a small, continuous increase up to very high injection currents (~ 1,222 A/cm^2), which has not been measured in previously reported nanowire LEDs.[17,27] Such unique characteristics can be well modeled using the ABF model, described by eq 1, for the LED internal quantum efficiency. Shown in Figure 5(a), variations of the calculated quantum efficiencies with current (solid curves) are in excellent agreement with the experimental results. The derived (A, B, C) values are (7.2×10^7 s^{-1}, 6.8×10^{-10} cm^{3}s^{-1}, 1.0×10^{-34} cm^{6}s^{-1}), (8.9×10^7 s^{-1}, 5.6×10^{-10} cm^{3}s^{-1}, 2.0×10^{-34} cm^{6}s^{-1}), and (9.6×10^7 s^{-1}, 3.9×10^{-10} cm^{3}s^{-1}, 3.0×10^{-34} cm^{6}s^{-1}) at 80 K, 200 K, and 300 K, respectively. While the values for A and B are reasonably close to those calculated for LED I, the values for C are nearly 5 orders of magnitude smaller, confirming the drastic reduction of electron overflow by the AlGaN electron blocking layer. These studies also strongly suggest that Auger recombination plays a very small, or negligible role on the performance of nanowire LEDs, since the

dx.doi.org/10.1021/nl203860b | Nano Lett. 2012, 12, 1317−1323

Auger coefficient (C) is expected to be relatively independent of the incorporation of an AlGaN electron blocking layer.

Finally, we have investigated InGaN/GaN dot-in-a-wire LEDs with the incorporation of an AlGaN electron blocking layer as well as the special technique of p-type modulation doping in the device active region. As demonstrated previously, the technique of p-type modulation doping can significantly improve the performance of nanowire LEDs by enhancing the hole injection and transport process in the quantum dot active region.[5,17] Variations of the relative external quantum efficiency with current density at room temperature are shown in Figure 5b. It is seen that the quantum efficiency first shows a significant rise (up to ~400 A/cm^2), followed by small, continuous increase at higher injection conditions. There is virtually no efficiency degradation for injection current density up to ~2200 A/cm^2. With the use of the ABF model, the values of A, B, and C are estimated to be ~2.7×10^8 s^{-1}, 4×10^{-10} cm^3 s^{-1}, and 1.0×10^{-34} cm^6 s^{-1}, respectively. Additionally, such dot-in-a-wire LEDs can exhibit highly stable white light emission. Locations of the light emission on the chromaticity diagram are shown in the inset of Figure 5b under various injection conditions (from ~333 to 1100 A/cm^2), with the values of x and y in the ranges of ~0.33−0.35 and 0.36−0.38, respectively. The extremely stable white light emission is attributed to the large inhomogeneous broadening of the dots, the highly uniform carrier distribution in the LED active region, and the drastically reduced QCSE in the nanowire heterostructures.

In summary, through extensive theoretical and experimental studies, we have demonstrated unambiguously that the maximum achievable quantum efficiency of GaN-based dot-in-a-wire LEDs is ultimately limited by electron leakage and overflow, rather than Auger recombination. Detailed temperature-dependent studies further confirm that efficiency droop in such nanowire LEDs becomes more severe at lower temperatures, which is directly correlated with the relatively enhanced electron overflow with decreasing temperature. We have further achieved for the first time an effective control of electron overflow in phosphor-free nanowire white LEDs by incorporating a p-doped AlGaN electron blocking layer between the quantum dot active region and the p-GaN. The resulting LEDs exhibit remarkably stable white light emission and are virtually free of any efficiency degradation up to ~2200 A/cm^2. This work has identified and addressed one of the major obstacles of nanowire LEDs for applications in future high-power phosphor-free, all-semiconductor based solid-state lighting.

■ ASSOCIATED CONTENT

Supporting Information

Simulation of the electron current density and carrier distribution of the InGaN/GaN dot-in-a-wire LED heterostructures. This material is available free of charge via the Internet at http://pubs.acs.org.

■ AUTHOR INFORMATION

Corresponding Author

*E-mail: zetian.mi@mcgill.ca. Phone: 1 514 398 7114.

Notes

The authors declare no competing financial interest.

■ ACKNOWLEDGMENTS

This work is being supported by the Natural Sciences and Engineering Research Council of Canada (NSERC), the Fonds de recherché sur la nature et les technologies, and McGill University. Part of the work was performed in the McGill University Micro Fabrication Facility. Electron microscopy images and analysis with the Titan 80-300 were carried out at the Canadian Centre for Electron Microscopy, a national facility supported by NSERC and McMaster University.

■ REFERENCES

(1) Kim, M. H.; Schubert, M. F.; Dai, Q.; Kim, J. K.; Schubert, E. F.; Piprek, J.; Park, Y. *Appl. Phys. Lett.* **2007**, *91*, 183507.
(2) Schubert, M. F.; Xu, J.; Kim, J. K.; Schubert, E. F.; Kim, M. H.; Yoon, S.; Lee, S. M.; Sone, C.; Sakong, T.; Park, Y. *Appl. Phys. Lett.* **2008**, *93*, 041102.
(3) Shen, Y. C.; Mueller, G. O.; Watanabe, S.; Gardner, N. F.; Munkholm, A.; Krames, M. R. *Appl. Phys. Lett.* **2007**, *91*, 141101.
(4) Zhang, M.; Bhattacharya, P.; Singh, J.; Hinckley, J. *Appl. Phys. Lett.* **2009**, *95*, 201108.
(5) Xie, J. Q.; Ni, X. F.; Fan, Q.; Shimada, R.; Ozgur, U.; Morkoc, H. *Appl. Phys. Lett.* **2008**, *93*, 121107.
(6) Monemar, B.; Sernelius, B. E. *Appl. Phys. Lett.* **2007**, *91*, 181103.
(7) Yang, Y.; Cao, X. A.; Yan, C. H. *IEEE Trans. Electron Devices* **2008**, *55*, 1771.
(8) Ozgur, U.; Ni, X.; Li, X.; Lee, J.; Liu, S.; Okur, S.; Avrutin, V.; Matulionis, A.; Morkoc, H. *Semicond. Sci. Technol.* **2011**, *26*, 014022.
(9) Ni, X.; Li, X.; Lee, J.; Liu, S.; Avrutin, V.; Ozgur, U.; Morkoc, H.; Matulionis, A.; Paskova, T.; Mulholland, G.; Evans, K. R. *Appl. Phys. Lett.* **2010**, *97*, 031110.
(10) Vampola, K. J.; Iza, M.; Keller, S.; DenBaars, S. P.; Nakamura, S. *Appl. Phys. Lett.* **2009**, *94*, 061116.
(11) Kikuchi, A.; Kawai, M.; Tada, M.; Kishino, K. *Jpn. J. Appl. Phys., Part 2* **2004**, *43*, L1524.
(12) Sekiguchi, H.; Kishino, K.; Kikuchi, A. *Appl. Phys. Lett.* **2010**, *96*, 231104.
(13) Qian, F.; Gradecak, S.; Li, Y.; Wen, C.; Lieber, C. *Nano Lett.* **2005**, *5*, 2287.
(14) Guo, W.; Zhang, M.; Banerjee, A.; Bhattacharya, P. *Nano Lett.* **2010**, *10*, 3355.
(15) Hong, C. C.; Ann, H.; Wu, C. Y.; Gwo, S. *Opt. Express* **2009**, *17*, 17227.
(16) Chang, Y. L.; Wang, J. L.; Li, F.; Mi, Z. *Appl. Phys. Lett.* **2010**, *96*, 013106.
(17) Nguyen, H. P. T; Zhang, S.; Cui, K.; Han, X.; Fathololoumi, S.; Couillard, M.; Botton, G. A.; Mi, Z. *Nano Lett.* **2011**, *11*, 1919.
(18) Barletta, P. T.; Berkman, E. A.; Moody, B. F.; El-Masry, N. A.; Emara, A. M.; Reed, M. J.; Bedair, S. M. *Appl. Phys. Lett.* **2007**, *90*, 151109.
(19) Damilano, B.; Grandjean, N.; Massies, J.; Siozade, L.; Leymarie, J. *Appl. Phys. Lett.* **2000**, *77*, 1268.
(20) Masui, H.; Sonoda, J.; Pfaff, N.; Koslow, I.; Nakamura, S.; DenBaars, S. P. *J. Phys. D: Appl. Phys.* **2008**, *41*, 165105.
(21) Qian, F.; Li, Y.; Gradečak, S.; Wang, D.; Barrelet, C. J.; Lieber, C. M. *Nano Lett.* **2004**, *4*, 1975.
(22) Kuykendall, T.; Ulrich, P.; Aloni, S.; Yang, P. *Nat. Mater.* **2007**, *6*, 951.
(23) Pope, I. A.; Smowton, P. M.; Blood, P.; Thomson, J. D.; Kappers, M. J.; Humphreys, C. J. *Appl. Phys. Lett.* **2003**, *82*, 2755.
(24) Van de Walle, C. G.; Segev, D. *J. Appl. Phys.* **2007**, *101*, 081704.
(25) Bertelli, M.; Loptien, P.; Wenderoth, M.; Rizzi, A.; Ulbrich, R. G.; Righi, M. C.; Ferretti, A.; Martin-Samos, L.; Bertoni, C. M.; Catellani, A. *Phys. Rev. B* **2009**, *80*, 115324.
(26) Bertazzi, F.; Goano, M.; Bellotti, E. *Appl. Phys. Lett.* **2010**, *97*, 231118.
(27) Guo, W.; Zhang, M.; Bhattacharya, P.; Heo, J. *Nano Lett.* **2011**, *11*, 1434.

(28) Ryu, H. Y.; Kim, H. S.; Shim, J. I. *Appl. Phys. Lett.* **2009**, *95*, 081114.
(29) Tu, R. C.; Tun, C. J.; Pan, S. M.; Chuo, C. C.; Sheu, J. K.; Tsai, C. E.; Wang, T. C.; Chi, G. C. *IEEE Photon. Technol. Lett.* **2003**, *15*, 1342.
(30) Kuo, Y. K.; Chang, Y. A. *IEEE J. Quantum Electron.* **2004**, *40*, 437.
(31) Nguyen, H. P. T; Cui, K.; Zhang, S.; Fathololoumi, S.; Mi, Z. *Nanotechnology* **2011**, *22*, 445202.
(32) Piprek, J.; Li, S. *Opt. Quantum Electron.* **2010**, *42*, 89.
(33) Dai, Q.; Shan, Q. F.; Wang, J.; Chhajed, S.; Cho, J.; Schubert, E. F.; Crawford, M. H.; Koleske, D. D.; Kim, M. H.; Park, Y. *Appl. Phys. Lett.* **2010**, *97*, 133507.
(34) Ling, S. C.; Lu, T. C.; Chang, S. P.; Chen, J. R.; Kuo, H. C.; Wang, S. C. *Appl. Phys. Lett.* **2010**, *96*, 231101.
(35) Chung, H. J.; Choi, R. J.; Kim, M. H.; Han, J. W.; Park, Y. M.; Kim, Y. S.; Paek, H. S.; Sone, C. S.; Park, Y. J.; Kim, J. K.; Schubert, E. F. *Appl. Phys. Lett.* **2009**, *95*, 241109.
(36) Meyaard, D. S.; Shan, Q.; Dai, Q.; Cho, J.; Schubert, E. F.; Kim, M.-H.; Sone, C. *Appl. Phys. Lett.* **2011**, *99*, 041112.
(37) Zhang, M.; Bhattacharya, P.; Singh, J.; Hinckley, J. *Appl. Phys. Lett.* **2009**, *95*, 201108.
(38) Meneghini, M.; Trivellin, N.; Meneghesso, G.; Zanoni, E.; Zehnder, U.; Hahn, B. J. *Appl. Phys.* **2009**, *106*, 114508.
(39) Chevtchenko, S.; Ni, X.; Fan, Q.; Baski, A. A.; Morkoc, H. *Appl. Phys. Lett.* **2006**, *88*, 122104.
(40) Bhattacharya, P.; Mi, Z. *Proc. IEEE* **2007**, *95*, 1723.
(41) Guo, W.; Banerjee, A.; Bhattacharya, P.; Ooi, B. S. *Appl. Phys. Lett.* **2011**, *98*, 193102.
(42) Ni, X.; Li, X.; Lee, J.; Liu, S.; Avrutin, V.; Özgür, Ü.; Morkoc, H.; Matulionis, A. J. *Appl. Phys.* **2010**, *108*, 033112.
(43) Ni, X.; Li, X.; Lee, J.; Liu, S.; Avrutin, V.; Ozgur, U.; Morkoc, H.; Matulionis, A.; Paskova, T.; Mulholland, G.; Evans, K. R. *Phys. Status Solidi RRL* **2010**, *4*, 194.
(44) Han, S. H.; Lee, D. Y.; Lee, S. J.; Cho, C. Y.; Kwon, M. K.; Lee, S. P.; Noh, D. Y.; Kim, D. J.; Kim, Y. C.; Park, S. J. *Appl. Phys. Lett.* **2009**, *94*, 231123.
(45) Rozhansky, I. V.; Zakheim, D. A. *Phys. Status Solidi A* **2007**, *204*, 227.
(46) Piprek, J. *Phys. Status Solidi A* **2010**, *207*, 2217.